J Appl Electrochem (2012) 42:477–482
DOI 10.1007/s10800-012-0422-4

ORIGINAL PAPER

# Investigation of immiscible Sn–Zn coatings with two-layer microstructure as anode material for Li-ion battery

**Zhijia Du · Shichao Zhang · Jianfeng Zhao · Yuan Fang**

Received: 27 February 2012 / Accepted: 23 April 2012 / Published online: 5 May 2012


**Abstract** The exfoliation of Sn as a result of volume expansion led to the drastic capacity decay in lithium-ion batteries. In this article, the immiscible Sn–Zn coating was successfully prepared by electrodeposition and applied as the anode material in Li-ion batteries. The physical structure and electrochemical properties were characterized by X-ray diffraction, scanning electron microscope, electron probe microanalysis and charge–discharge test, respectively. The Sn–Zn deposit displayed unique two-layer morphology composed of a Zn flat bottom layer and a Sn dendritic upper layer. The novel Sn–Zn electrodes showed noticeable improvement in cyclability compared to pure Sn film. This improvement was assigned to the characteristic of the two-layer microstructure: the Zn interlayer enhanced the binding strength between Sn dendrites and copper foil; the abundant space among these individual Sn dendrites accommodated the volume expansion during lithiation process. The two-layer Sn–Zn coatings were anticipated as potential anode materials for Li-ion batteries.

**Keywords** Li-ion batteries · Anode materials · Sn–Zn coatings · Electrodeposition

## 1 Introduction

The development of high capacity and long lifespan lithium-ion batteries has motivated worldwide research efforts in the last two decades [1, 2]. Tin has been extensively investigated to replace graphite as anode material owing to its high theoretical capacity of 994 mAh $g^{-1}$ (corresponding to the formula of $Li_{22}Sn_5$) [3, 4]. However, earlier research revealed that Sn underwent fierce volume variation during lithiation/delithiation process, which resulted in severe structural exfoliation and electrical degradation [3, 5]. Consequently, drastic capacity decay occurred and thereby obstructed the practical implementation of tin as anode materials in Li-ion batteries.

To conquer this difficulty, one effective scheme is turning to tin-based intermetallics or composites to cushion the volume expansion and obtain good cycle performance. The principal concept of preferring intermetallics or composites to pure tin is that: Sn reacts with Li to form the $Li_xSn$ alloy in lithiation process, whereas the other component serves as the inactive confining matrix to buffer the volume expansion of $Li_xSn$ [3]. Various tin-based intermetallics have been recommended as the anode materials such as Sn–Cu [6], Sn–Fe [7], Sn–Ni [8], Sn–Co [9], etc. However, there are only a few reports about the immiscible tin-based materials such as Sn–Zn composite. In previous report, Zn was thought to strengthen the interface adhesion between the plated Sn film and the Cu foil without forming a stable lithiated compound [10]. The Sn–Zn film deposited on Cu foil showed certain improvement in cycle stability.

Another promising approach to improve the cyclability of tin-based electrodes is to design specific nanostructured electrode as discussed in previous report [11, 12]. These electrode configurations enlarged the effective surface area of the electrode; meanwhile there was adequate space to accommodate the volume expansion of active materials during repeat charge/discharge process.

In this study, immiscible Sn–Zn thin film with two-layer microstructure was prepared by electrodeposition, which

Z. Du · S. Zhang (✉) · J. Zhao · Y. Fang
School of Materials Science and Engineering, Beihang University, XueYuan Road No. 37, HaiDian District, Beijing 100191, People's Republic of China
e-mail: csc@buaa.edu.cn; labofcsc@gmail.com

Z. Du
e-mail: duzhijia@mse.buaa.edu.cn

showed improvement of cyclability in Li-ion batteries. In the Sn–Zn coatings, the bottom layer was a compact Zn-dominant deposit while the upper layer was composed of many Sn dendrites. The electrodeposition mechanism was discussed briefly in the report. Eventually, the good electrochemical behavior of the electrode was displayed, and the probable mechanism was investigated.

## 2 Experimental description

The electrodes were prepared by electrodepositing Sn–Zn coatings onto copper foils. The composition of the electrolytic bath was listed in Table 1. The electrolytic solution was continually stirred by a magnetic bar with Pt foil as anode during electrodeposition. To determine the electroreduction potential of each metal cation, cyclic voltammetry (CV) experiments were performed at 50.0 mV $s^{-1}$ via a Zahner electrochemical workstation (iM6ex). Sn and Sn–Zn deposits used in the lithium-ion batteries test were obtained potentiostatically at −1.3 V for 120 s under room temperature. The mass of the thin films was calculated by measuring the substrates before and after electrodeposition via a METTLER AB135-S analytical balance.

The morphologies, composition, and phase structure of the electrodes were investigated by field emission scanning electron microscopy (FE-SEM, Hitachi S-4800 SEM system), electron probe microanalysis (EPMA), and MAC Science X-ray diffraction (XRD) (Cu Kα radiation), respectively.

Electrochemical charge–discharge behaviors were investigated in half-cells assembled with the as-prepared anodes, lithium foils, and Celgard 2300 membranes in an Ar-filled glove box (MB-10-G with TP170b/mono, MBRAUN). 1 M $LiPF_6$/EC − DEC (1:1 by vol%) was used as the electrolyte. Each cell was aged for 20 h at room temperature before commencing the electrochemical tests. The galvanostatic charge–discharge measurements were carried out in a battery test system (NEWARE BTS-610, Newware Technology Co., Ltd., China) at room temperature with cut-off voltage of 0.01–1.5 V.

**Table 1** Composition of the electrolytic solution for Sn–Zn coatings electrodeposition

| Bath | $SnSO_4$ mol $L^{-1}$ | $ZnSO_4{\cdot}7H_2O$ mol $L^{-1}$ | $Na_2SO_4$ mol $L^{-1}$ | Tartaric acid mol $L^{-1}$ |
|---|---|---|---|---|
| A | 0.02 | – | 1.0 | 0.12 |
| B | – | 0.02 | 1.0 | 0.12 |
| C | 0.02 | 0.02 | 1.0 | 0.12 |

## 3 Results and discussion

To fix the electrodeposition potential of Sn and Zn, CV tests were performed in the electrolytic bath A, B and C, which were shown in Fig. 1. The cathodic peak at −0.6 V in bath A was ascribed to the reduction of stannous ion. The location of this peak related to $Sn^{2+}$ reduction was hardly changed when zinc chloride was added in bath C. For bath B, there was no obvious cathodic peak in the negative scanning process, but a slope ranging from −0.9 to −1.2 V corresponding to the reduction of $Zn^{2+}$. Similarly, the location of the $Zn^{2+}$ reduction slope was hardly varied when stannous chloride was added in bath C, which indicated that the reduction potential of $Zn^{2+}$ was more negative than that of $Sn^{2+}$. Based on the above analysis, the electrodeposition potential of Sn–Zn coatings was set at −1.3 V.

To confirm the phase structure of the electrodeposited Sn–Zn coatings, XRD measurement was performed as shown in Fig. 2. The three high intensity peaks were simply assigned to the copper foil. The peak at 30.6° was in

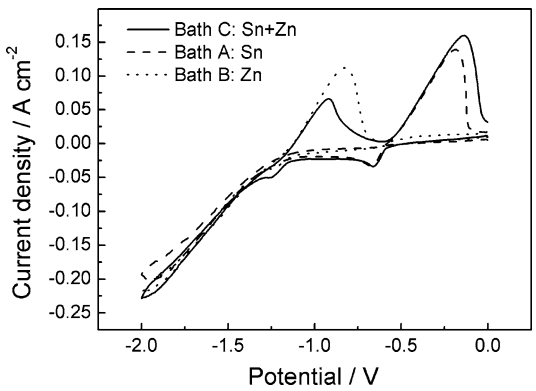


**Fig. 1** Cyclic voltammograms of a copper foil in bath A, B, and C

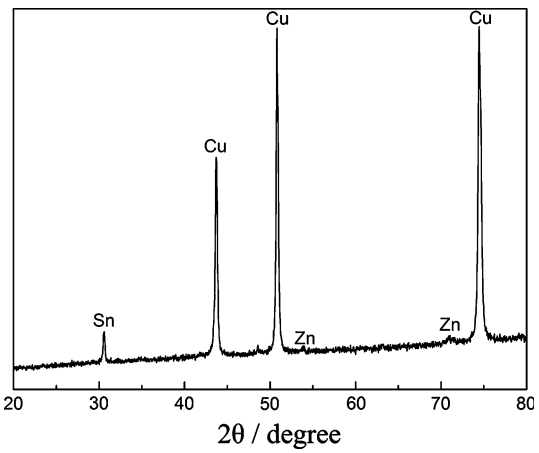


**Fig. 2** XRD pattern of the Sn–Zn coatings

accordance with (200) of $\beta$-Sn phase, and the unobvious peaks at 54.2° and 70.9° were in agreement with (102) and (110) of Zn phase, respectively. The previous reported Sn–Zn thermal phase diagram revealed that the mutual solubility of Sn and Zn was very low and intermetallic formation was thought to be thermo-dynamically impossible [13]. It is obvious that our XRD results also supported this conclusion.

The SEM images of the Sn–Zn and Sn coatings were shown in Fig. 3a and b, respectively. It revealed that the as-deposited Sn–Zn coatings were composed of two different layers. The bottom layer was comparatively flat with dense packed crystallites, while the upper layer showed many mutually independent dendritic crystallites which came up from the bottom layer as presented in the inset of Fig. 3a. However, the as-deposited Sn coatings showed no distinct feature but smooth sediment.

Furthermore, EPMA was carried out to further investigate the elemental distribution maps of the two-layer Sn–Zn coatings as displayed in Fig. 4. The macro segregation of Sn and Zn was observed in combination with the morphology variation of the coatings. Basically, Sn mainly existed in the dendrites of the upper layer while Zn showed the aggregation dominantly in the flat bottom layer. To further verify this elemental distribution, a corrosion experiment was carried out on the Sn–Zn coatings as reported before [14]. The etching solution was composed of 93 % methanol, 5 % nitric acid and 2 % hydrochloric acid. The etching time was set at 5 min with most of the deposit corroded away. The SEM image of the coatings after chemical etching in Fig. 5a showed only a flat layer without any dendrite. The EDX spectrogram in Fig. 5b revealed that all of Sn was corroded away because only Zn and Cu signals were observed. Therefore, it was demonstrated that there was a Zn interlayer between the deposited coatings and the copper foil.

From the above discussion, it was concluded that $Zn^{2+}$ might be favorable to be electrodeposited rather than $Sn^{2+}$. However, this phenomenon was somewhat disobedient to the CV results obtain in solution C in which the reduction potential of $Zn^{2+}$ was more negative than that of $Sn^{2+}$. This behavior was probably assigned to the anomalous codeposition mechanism which often occurred in co-electrodeposition related with Zn [15]. This unique microstructure of the coatings with Zn interlayer and independent Sn dendrites played an important role in enhancing the cycle performance of Sn-based anode, which would be discussed later.

The as-deposited Sn and Sn–Zn coatings were directly assembled into half-cells with no other binding or conductive additives to investigate their Li-storage properties. Figure 6a and c showed the voltage profiles of Sn and Sn–Zn electrodes, respectively, cycled over a voltage range of 0.01–1.5 V at 0.2 C. Obviously, the Sn and Sn–Zn electrodes presented similar discharge–charge profiles which were consistent with previous report on pure Sn anodes [4]. Three plateaus were observed during discharge at $\sim$0.66, 0.49 and 0.38 V as a consequence of lithiation potential of Sn, $Li_2Sn_5$, and LiSn, respectively. The subsequent sloping region gradually dropping to 0.01 V was related to the further lithiation of LiSn to form successive Li-rich phases $Li_xSn_y$. Both Sn and Sn–Zn electrodes displayed irreversible capacity above 0.7 V, which probably resulted from the formation of solid electrolyte interphase (SEI) layers and/or the reduction of possible oxide impurities on electrode surface [16, 17]. The plateaus observed during charge were attributed to the Li extraction from a series of $Li_xSn_y$ alloys. The plots of differential capacity with potential for the as-deposited Sn and Sn–Zn coatings are displayed in Fig. 6b and d, respectively. The peaks in the plots better elucidate the reaction mechanism between lithium and as-deposited coatings. This similar profile characteristic demonstrated that in the as-deposited Sn–Zn coatings, the Sn and Zn existed as primary phase with a weak interaction between them. Therefore, the Sn–Zn electrode showed only the Sn–Li alloying specificity.

Figure 7a depicted the reversible capacity and Coulombic efficiency versus cycle number plots, rendering a

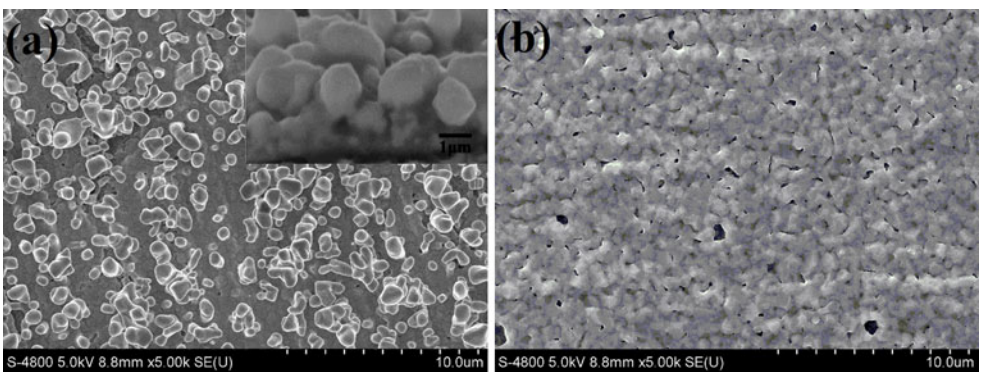


**Fig. 3** **a** Top and cross-sectional (*inset*) SEM images of the as-deposited Sn–Zn coatings. **b** Top SEM images of the as-deposited Sn coatings

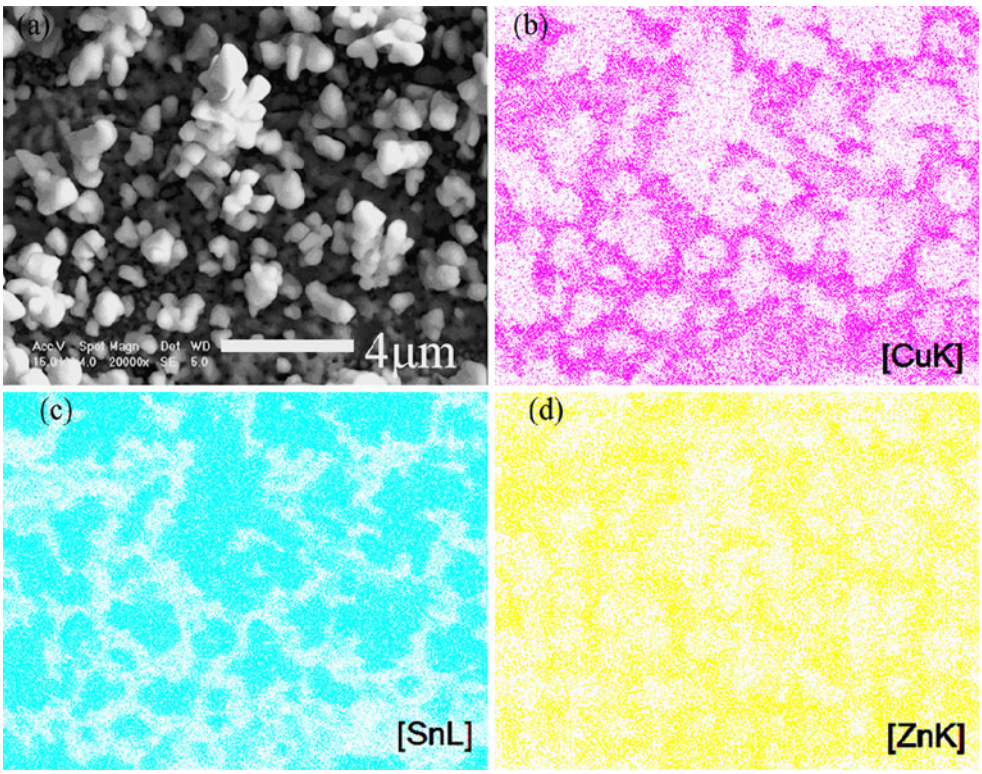


**Fig. 4** **a** SEM image of as-deposited Sn–Zn coatings. **b**, **c**, **d** Compositional Cu, Sn, and Zn maps scanned by EPMA

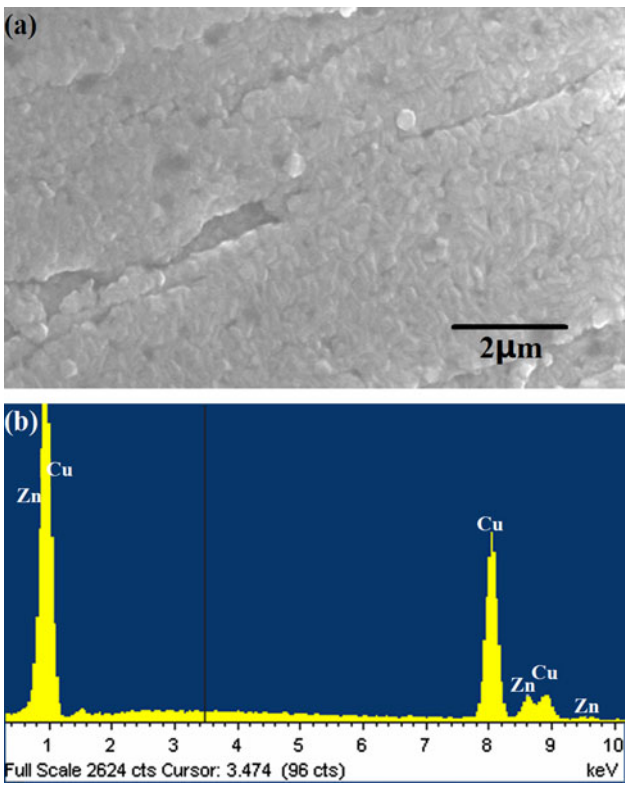


**Fig. 5** **a** SEM image and **b** EDX spectrogram of Sn–Zn coatings after etching for 5 min

direct evidence of the superior cyclability of two-layer Sn–Zn coatings to pure Sn. For the as-deposited Sn anode, the first charge capacity was 768 mAh $g^{-1}$ and the capacity for the 15th cycle was 779 mAh $g^{-1}$, indicating that the cycling performance in the first 15 cycles was fairly good. However, the charge capacity subsequently decayed drastically to 195 mAh $g^{-1}$ for the 30th cycle, leaving retention rate of merely 25.4 % which was certainly unusable for commercial application. However, the two-layer Sn–Zn anode performed well in the entire 30 cycles. The first charge capacity was 673 mAh $g^{-1}$ smaller than that of Sn anode, because the introduction of Zn into the tin-based coating lowered the proportion of Sn. The charge capacity for the 30th cycle was 552 mAh $g^{-1}$, providing retention rate of 82 %. Figure 7b displayed the rate capability of Sn–Zn coatings with the rate increased stepwise up to 3 C. The electrode delivered a satisfying fraction of its initial capacity and carried on with a stable cycling response at each stage. For instance, the capacity retention rates at 2 C and 3 C are 64.6 and 58.2 % compared to the 0.2 C capacity, respectively.

The reason why the Li-storage performance was improved might be probably ascribed to the unique two-layer microstructure of the Sn–Zn coatings. First, the segregated Zn interlayer strengthened the interface contact between the active material and copper foil [18]. Thus, the

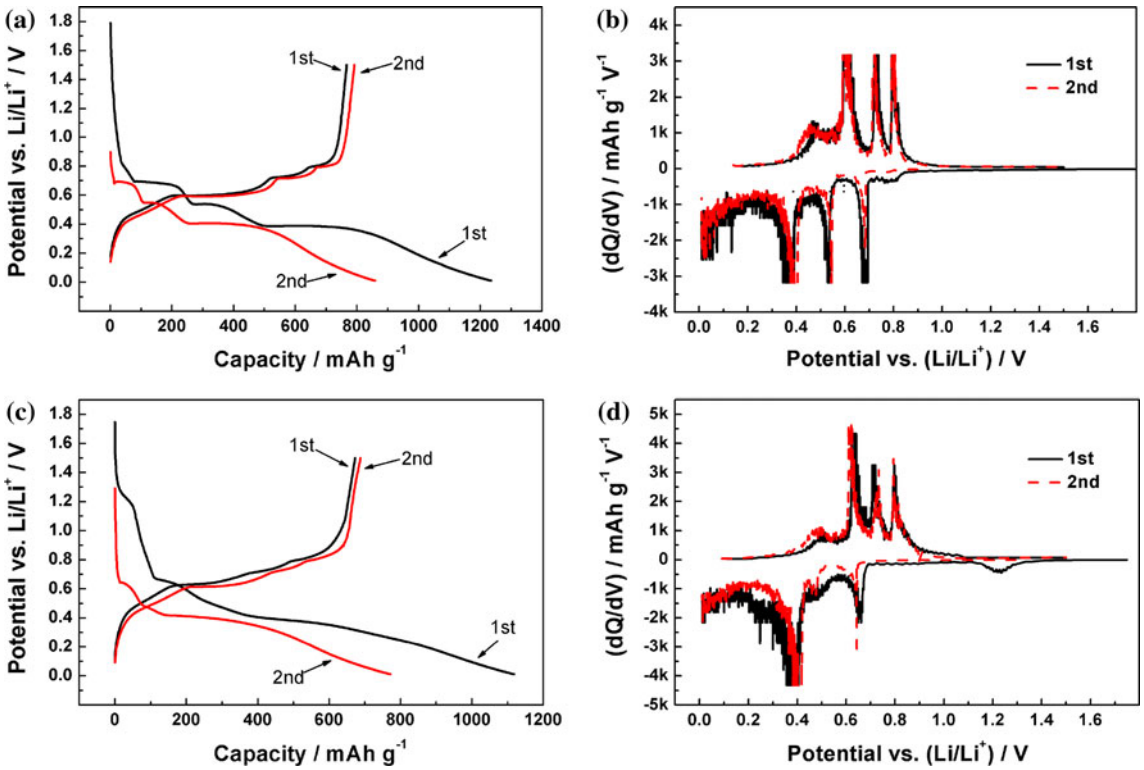


**Fig. 6** **a**, **b** Voltage profiles and differential capacity with potential of the as-deposited Sn anode. **c**, **d** Voltage profiles and differential capacity with potential of the as-deposited Sn–Zn anode

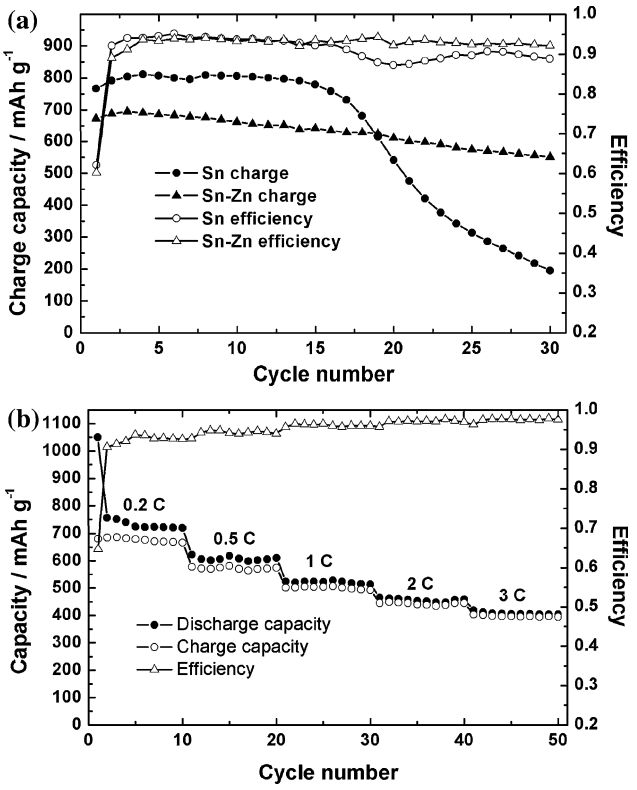


**Fig. 7** **a** Reversible capacity and Coulombic efficiency versus cycle number for the as-deposited Sn anode and as-deposited Sn–Zn anode. **b** Cycle performance of the Sn–Zn coatings at different rates

active material delaminating from copper foil was considerably prevented during cyclic lithiation/delithiation. Second, there was substantial space between the adjacent Sn dendrites in the upper layer, which was capable of accommodating the volume expansion of Sn during discharge process. Finally, the certain amount of Zn element existed in Sn dendrites formed a multiphase active/inactive composite in which Zn phase functioned as the cushion to buffer the internal strain in the Sn-rich dendrites. Therefore, the electrodeposited immiscible Sn–Zn coatings with unique two-layer microstructure represented a promising approach to enhance the cyclability of tin-based electrode.

## 4 Conclusion

The co-electrodeposition behavior of Sn–Zn coatings was investigated, and unique two-layer Sn–Zn coatings were prepared successfully via electrodeposition. The XRD pattern revealed that the Sn–Zn coatings belonged to the immiscible system without any intermetallics. The segregation of Sn and Zn evolved a special two-layer microstructure with a Sn dendrites upper layer and a Zn flat bottom layer. The first reversible capacity of Sn–Zn coatings was 673 mAh $g^{-1}$ and the retention rate was 82 % after 30 cycles. This improvement of cycle performance

was attributed to the synergetic effect of the interfacial enhancement by Zn interlayer, the accommodation for volume expansion by empty space, and the internal stress buffer by Zn phase particles. Therefore, the unique Sn–Zn coatings with two-layer microstructure were promising candidates as the anode materials in lithium-ion batteries.

**Acknowledgments** This study was supported by the National Natural Science Foundation of China (50954005, 51074011), National Basic Research Program of China (2007CB936502) and National 863 Program (2006AA03Z230 and 2008AA03Z208), and the Scholarship Award for Excellent Doctoral Student granted by China Ministry of Education.

## References

1. Goodenough JB, Kim Y (2010) Challenges for rechargeable Li batteries. Chem Mater 22:587
2. Armand M, Tarascon JM (2008) Building better batteries. Nature 451:652
3. Winter M, Besenhard JO (1999) Electrochemical lithiation of tin and tin-based intermetallics and composites. Electrochim Acta 45:31
4. Courtney IA, Tse JS, Mao O, Hafner J, Dahn JR (1998) Ab initio calculation of the lithium-tin voltage profile. Phys Rev B 58: 15583
5. Beaulieu LY, Beattie SD, Hatchard TD, Dahn JR (2003) The electrochemical reaction of lithium with tin studied by in situ AFM. J Electrochem Soc 150:A419
6. Wang F, Zhao M, Song X (2007) Influence of the preparation conditions on the morphology and electrochemical performance of nano-sized Cu–Sn alloy anodes. J Alloys Compd 439:249
7. Zhang CQ, Tu JP, Huang XH, Yuan YF, Wang SF, Mao F (2008) Preparation and electrochemical performances of nanoscale $FeSn_2$ as anode material for lithium ion batteries. J Alloys Compd 457:81
8. Du Z, Zhang S, Xing Y, Wu X (2011) Nanocone-arrays supported tin-based anode materials for lithium-ion battery. J Power Sources 196:9780
9. Ferrara G, Damen L, Arbizzani C, Inguanta R, Piazza S, Sunseri C, Mastragostino M (2011) SnCo nanowire array as negative electrode for lithium-ion batteries. J Power Sources 196:1469
10. Wang L, Kitamura S, Obata K, Tanase S, Sakai T (2005) Multilayered Sn–Zn–Cu alloy thin-film as negative electrodes for advanced lithium-ion batteries. J Power Sources 141:286
11. Hassoun J, Panero S, Simon P, Taberna PL, Scrosati B (2007) High-rate, long-life Ni–Sn nanostructured electrodes for lithium-ion batteries. Adv Mater 191:632
12. Zhang S, Du Z, Lin R, Jiang T, Liu G, Wu X, Weng D (2010) Nickel nanocone-array supported silicon anode for high-performance lithium-ion batteries. Adv Mater 22:5378
13. Vnuk F, Ainsley MH (1981) The solid solubility of silver, gold and zinc in metallic tin. J Mater Sci 16:1171
14. Wu CML, Yu DQ, Law CMT, Wang L (2002) The properties of Sn-9Zn lead-free solder alloys doped with trace rare earth elements. J Electron Mater 31:921
15. Landolt D (1994) Electrochemical and materials science aspects of alloy deposition. Electrochim Acta 39:1075
16. He J, Zhao H, Wang J, Wang J, Chen J (2010) Hydrothermal synthesis and electrochemical properties of nano-sized Co–Sn alloy anodes for lithium ion batteries. J Alloys Compd 508:629
17. Todd ADW, Mar RE, Dahn JR (2006) Combinatorial study of tin-transition metal alloys as negative electrodes for lithium-ion batteries. J Electrochem Soc 153:A1998
18. Wang L, Kitamura S, Sonoda T, Obata K, Tanase S, Sakai T (2003) Electroplated Sn–Zn alloy electrode for Li secondary batteries. J Electrochem Soc 150:A1346